Available online at www.sciencedirect.com
SCIENCE DIRECT®
International Journal of Mass Spectrometry 233 (2004) 25–31
International Journal of Mass Spectrometry
www.elsevier.com/locate/ijms

Measurements of absolute total and partial cross sections for the electron ionization of tungsten hexafluoride (WF_6)

R. Basner [a,*], M. Schmidt [a], K. Becker [b,c]

[a] *Institut für Niedertemperatur-Plasmaphysik, Friedrich-Ludwig-Jahn-Strasse 19, Ernst-Moritz-Arndt-Universitat, Greifswald D-17489, Germany*
[b] *Department of Physics and Engineering Physics, Stevens Institute of Technology, Hoboken, NJ 07030, USA*
[c] *Center for Environmental Systems, Stevens Institute of Technology, Hoboken, NJ 07030, USA*

Received 18 September 2003; accepted 6 October 2003

Abstract

We measured absolute partial cross sections for the formation of positive ions followed by electron impact on tungsten hexafluoride (WF_6) from threshold to 900 eV using a time-of-flight mass spectrometer (TOF-MS). Dissociative ionization processes resulting in seven different singly charged ions (F^+, W^+, WF_x^+, $x = 1$–5) and five doubly charged ions (W^{2+}, WF_x^{2+}, $x = 1$–4) were found to be the dominant ionization channels. The ion spectrum at all impact energies is dominated by WF_5^+ fragment ions. At 120 eV impact energy, the partial WF_5^+ ionization cross section has a maximum value of 3.92×10^{-16} cm^2 that corresponds to 43% of the total ion yield. The cross section values of all the other singly charged fragment ions at 120 eV range between 0.39×10^{-16} and 0.73×10^{-16} cm^2. The ionization cross sections of the doubly charged ions are more than one order of magnitude lower than the cross section of WF_5^+. Double ionization processes account for 21% of the total ion yield at 120 eV. The absolute total ionization cross section of WF_6 was obtained as the sum of all measured partial ionization cross sections and is compared with available calculated cross sections.

Keywords: Tungsten hexafluoride; Electron ionization; Cross sections; Plasma processing

1. Introduction

Plasma-enhanced chemical vapor deposition processes are an important area of application of non-thermal, low-pressure plasmas. In these plasmas, ionization and dissociative ionization of the neutral heavy particles in the ground or in excited states by electron impact is an important and, in many plasmas, the dominant ion and radical formation process depending on the shape of the electron energy distribution function. In an effort to understand the electron ionization processes and to develop models of the chemistry occurring in technologically important plasmas various reliable cross sections for the electron impact ionization and dissociative ionization are needed. Tungsten hexafluoride (WF_6) is widely used as a precursor for plasma-enhanced deposition of tungsten-containing thin films in materials processing for mechanical surface protection [1–3] and in the fabrication of microelectronic devices [4–6].

Our group reported the first experimentally determined electron ionization cross sections for WF_6 more than 10 years ago in a Conference report [7]. The data were obtained using a sector-field mass spectrometer with a very high mass resolution. Measurements carried out with this instrument were highly susceptible to ion discrimination, i.e., fragment ions with excess kinetic energy were not detected with 100% efficiency. Moreover, it was not possible to carry out a complete quantitative correction of this ion loss. Therefore, the data were never published in a peer-reviewed journal. Here, we report measured electron ionization cross section data for WF_6 obtained in a time-of-flight mass spectrometer (TOF-MS) that allows us to determine reliable absolute partial ionization cross sections without mass discrimination of the energetic fragment ions.

2. Experimental details

The measurements were carried out using a TOF-MS that is shown schematically in Fig. 1. The instrument and the data acquisition and analysis procedures have been described in

* Corresponding author. Tel.: +49-3834-554-426; fax: +49-3834-554-301.
E-mail address: basner@inp-greifswald.de (R. Basner).

1387-3806/$ – see front matter © 2004 Elsevier B.V. All rights reserved.
doi:10.1016/j.ijms.2003.10.014

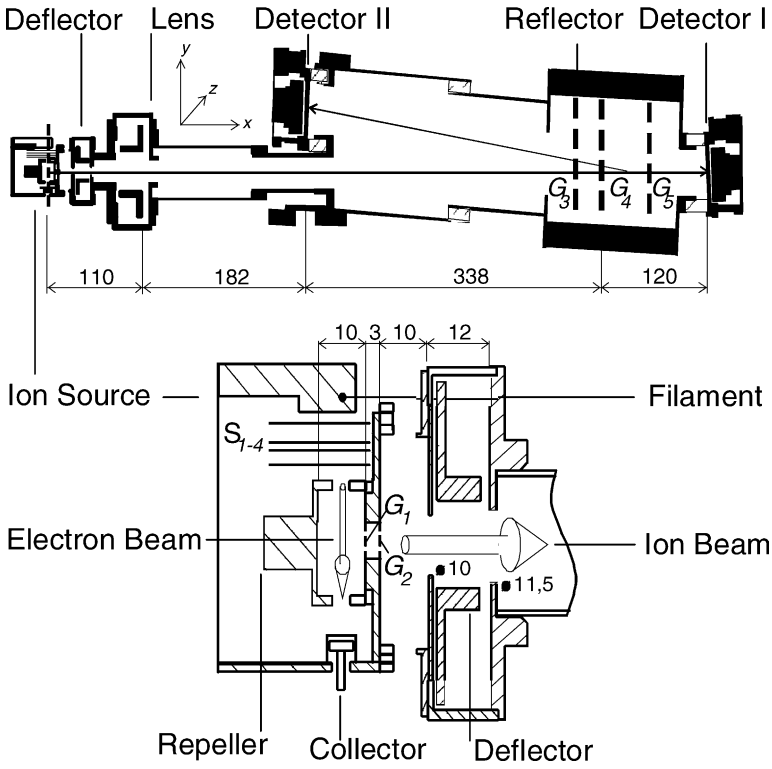

Fig. 1. Schematic diagram of the TOF-MS and a detailed view of the electron impact ion source used in the present study (all dimensions are in millimeters).

detail before [8–10] and the reliability of this mass spectrometric technique for the measurement for absolute partial ionization cross sections of energetic fragment ions was demonstrated in the case of $TiCl_4$, SiF_4, and C_2F_6 [8–10]. Briefly, the TOF-MS can be operated either in a linear mode using detector I or in a reflection mode using the reflector (grids: G_3, G_4, G_5) and detector II. In the present study, all measurements for the determination of the partial ionization cross sections were performed with the TOF-MS operated in the linear mode to ensure complete ion transport from the ion source to the detector and to reduce the data collection time by operating the instrument at a maximum repetition frequency of 20 kHz. The ion source chamber was filled with a well-defined WF_6/Ar mixture through precision leak valves up to partial pressures of about 1×10^{-4} Pa in an effort to facilitate the simultaneous measurements of the ions from WF_6 and Ar under identical operating conditions. The relative partial WF_6 ionization cross sections were put on an absolute scale by normalization relative to the partial Ar^+ ionization cross section of 2.52×10^{-16} cm^2 at 70 eV [11]. Taking into account the uncertainties of ±5% in the Ar reference cross section [11], the statistical uncertainty in our pressure measurement of ±3% and an uncertainty of typically ±3–7% resulting from the counting statistics, we assign an overall uncertainty of ±15% to the absolute ionization cross sections reported here.

Typically, the electron gun was operated using electron pulses of 100 ns width. The electron beam has a diameter of about 0.6 mm in the interaction region and the amplitude of the electron pulse was in the range from 1 to 10 μA with an energy spread of about 0.5 eV (FWHM). The impact energy was varied from 5 to 900 eV and the electron beam was guided by a weak magnetic field (200 G). A voltage of 1 kV (extraction fields of 1 kV cm^{-1}) was applied to the repeller, roughly 10 ns after the incident electron pulse passed through the ionization region. This extraction pulse accelerates the ions formed by electron impact toward the grounded ion source exit aperture and the entrance electrode of the flight tube, which is held at a −2.8 kV bias voltage. We maintained operating conditions under which 100% ion transmission of all ions from the ion source to the detector was established with the exception of ion losses at the grids G_1 and G_2. The output signal from the respective MCP passes a preamplifier, a constant fraction discriminator and is recorded with a 2 GHz multiscaler (FAST ComTec, Model 7886) with a time resolution of 500 ps. Our TOF-MS was operated in such a way that no more than one ion of the most intense ion signal was created during each electron pulse. This resulted in low overall count rates and comparatively long data acquisition times, but ensured, on the other hand, that dead time corrections to the recorded signal rates were negligible.

3. Results and discussions

The mass spectra of ions resulting from electron impact on WF_6 at an electron energy of 70 eV derived from measurements carried out with the TOF-MS operated in the lin-

ear mode and in reflection mode were found to be identical. In the reflection mode, with the much higher mass resolution, the five isotopic contributions of tungsten are completely separated for all fragment ions and correspond to the excepted values [12]. Our results are in excellent agreement with the mass spectra found in the NIST data base [13] for the heavier ions WF_5^+ and WF_4^+, but we found significantly higher ion signals for WF_3^+ (by 14%), WF_2^+ (by 29%), WF^+ (by 39%), and W^+ (by 31%), respectively. The reason for this discrepancy may be the optimized detection efficiency of our TOF-MS for energetic fragment ions. This optimization is usually not done for quadrupole mass spectrometers that are commonly used in analytic mass spectrometry. We carried out qualitative checks of the excess kinetic energy for all fragment ions by performing a full horizontal sweep of the extracted ion beam using a double-focusing mass spectrometer and comparing the shapes with the Ar^+ ion signal, which is characteristic of a beam of ions without excess kinetic energy [8,14,15]. All curves show a broadening which is indicative of excess kinetic energy. The broadening for the ions WF_5^+ and WF_4^+ is small and nearly identical and indicates only a small amount of excess kinetic energy. The broadening increases from WF_3^+ to WF_2^+ to WF^+ to W^+. A similar broadening pattern was found for the doubly charged fragment ions. By far the strongest broadening was measured for the light F^+ fragment ion, which is indicative of a broad distribution of excess kinetic energies. The WF_6 mass spectrum in the NIST data base [13] does not show any F^+ signal at all. As stated above, all data reported here were obtained under operating conditions that guarantee 100% ion transmission of all ions from the ion source to the detector was established with the exception of minor ion losses at the grids G_1 and G_2.

We found no evidence of thermal decomposition of WF_6 at the hot surface of the filament used in the electron gun. The measured threshold for the F^+ ions at about 23 eV (Table 1) is much higher than the ionization energy of atomic F (17.422 eV [16]) and the appearance energy of F^+ from F_2 (15.6 eV [16]). This demonstrates that the entire recorded F^+ ion signal can be attributed to F^+ fragment ions resulting from the dissociative ionization of WF_6.

Table 1
Absolute partial counting and total (charge weighted) electron ionization cross sections for WF_6 as a function of electron energy

Electron energy (eV)	Ionization cross section (10^{-16} cm^2)						
	Ion						
	F^+	W^+	WF^+	WF_2^+	WF_3^+	WF_4^+	WF_5^+
16							0.0059
17							0.103
18							0.228
19							0.328
20						0.00271	0.455
21						0.0077	0.62
22						0.013	0.755
23	0.0021					0.034	0.915
24	0.0047					0.055	1.04
25	0.0061					0.079	1.18
26	0.0082				0.0053	0.116	1.35
27	0.012				0.017	0.162	1.52
28	0.014				0.036	0.196	1.63
29	0.016				0.063	0.235	1.76
30	0.019				0.09	0.275	1.87
31	0.024			0.0021	0.143	0.316	2.07
32	0.031			0.0049	0.203	0.351	2.17
34	0.038			0.041	0.28	0.417	2.46
36	0.051			0.096	0.339	0.452	2.62
38	0.061			0.183	0.397	0.478	2.74
40	0.071		0.012	0.245	0.434	0.497	2.84
42	0.082		0.033	0.294	0.457	0.505	2.9
44	0.091		0.067	0.339	0.482	0.51	2.98
46	0.102	0.0033	0.105	0.389	0.506	0.513	3.05
48	0.108	0.01	0.14	0.426	0.528	0.515	3.12
50	0.117	0.034	0.173	0.473	0.548	0.519	3.19
55	0.151	0.091	0.216	0.529	0.561	0.522	3.33
60	0.179	0.143	0.262	0.565	0.564	0.524	3.44
65	0.212	0.176	0.289	0.596	0.566	0.523	3.54
70	0.258	0.21	0.32	0.633	0.566	0.523	3.62
80	0.357	0.286	0.36	0.689	0.559	0.52	3.75
90	0.461	0.346	0.381	0.703	0.548	0.517	3.86

Table 1 (*Continued*)

Electron energy (eV)	Ionization cross section (10^{-16} cm^2)						
	Ion						
	F^+	W^+	WF^+	$WF_2{}^+$	$WF_3{}^+$	$WF_4{}^+$	$WF_5{}^+$
100	0.566	0.392	0.387	0.701	0.535	0.514	3.91
120	0.731	0.444	0.387	0.677	0.502	0.505	3.92
140	0.874	0.472	0.383	0.653	0.478	0.488	3.91
160	0.999	0.489	0.375	0.62	0.446	0.477	3.86
180	1.07	0.497	0.366	0.598	0.417	0.466	3.82
200	1.08	0.497	0.359	0.573	0.405	0.459	3.77
300	1.02	0.449	0.309	0.488	0.332	0.422	3.47
400	0.897	0.373	0.261	0.407	0.288	0.379	3.08
500	0.728	0.309	0.221	0.352	0.241	0.329	2.75
600	0.628	0.277	0.201	0.305	0.212	0.288	2.53
700	0.552	0.237	0.179	0.272	0.18	0.267	2.27
800	0.502	0.214	0.162	0.243	0.167	0.254	2.09
900	0.457	0.187	0.143	0.228	0.155	0.24	1.96
	W^{++}	WF^{++}	$WF_2{}^{++}$	$WF_3{}^{++}$	$WF_4{}^{++}$	Total	
16						0.0059	
17						0.103	
18						0.228	
19						0.328	
20						0.458	
21						0.628	
22						0.768	
23						0.9511	
24						1.01	
25						1.27	
26						1.48	
27						1.71	
28						1.88	
29						2.07	
30						2.25	
31						2.55	
32						2.76	
34						3.24	
36						3.56	
38						3.86	
40						4.1	
42					0.00175	4.27	
44					0.00606	4.48	
46					0.01307	4.69	
48				0.0021	0.02	4.89	
50				0.0048	0.033	5.13	
55			0.0053	0.021	0.06	5.57	
60		0.0024	0.019	0.043	0.089	5.98	
65	0.0022	0.012	0.032	0.059	0.11	6.33	
70	0.013	0.027	0.052	0.083	0.136	6.75	
80	0.063	0.071	0.102	0.124	0.183	7.61	
90	0.101	0.101	0.135	0.162	0.228	8.27	
100	0.135	0.123	0.154	0.183	0.249	8.69	
120	0.18	0.15	0.174	0.208	0.268	9.13	
140	0.219	0.169	0.191	0.219	0.279	9.41	
160	0.237	0.173	0.195	0.23	0.282	9.5	
180	0.247	0.173	0.192	0.232	0.281	9.48	
200	0.249	0.171	0.191	0.231	0.281	9.39	
300	0.235	0.154	0.175	0.217	0.255	8.56	
400	0.194	0.125	0.152	0.187	0.212	7.42	
500	0.157	0.101	0.126	0.164	0.178	6.38	
600	0.142	0.089	0.109	0.149	0.156	5.73	
700	0.119	0.077	0.098	0.135	0.134	5.08	
800	0.102	0.069	0.085	0.12	0.118	4.62	
900	0.092	0.061	0.08	0.114	0.105	4.27	

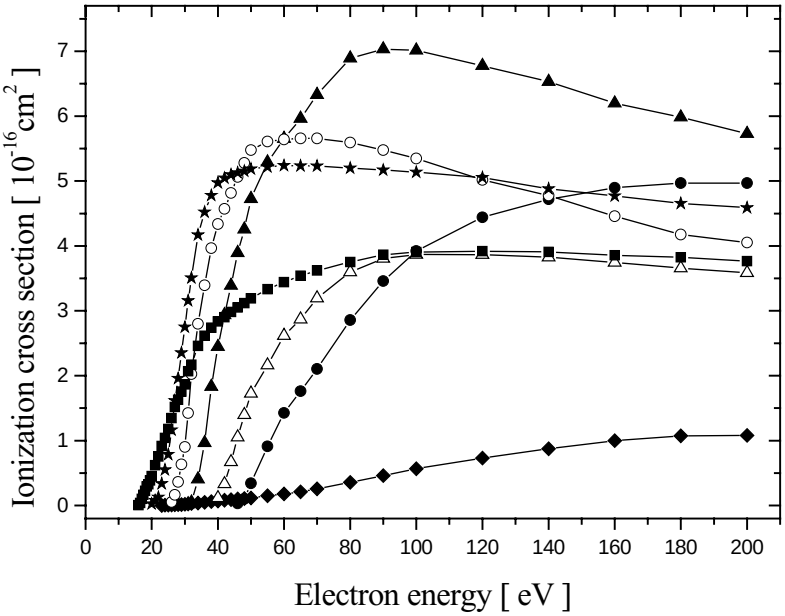

Fig. 2. Absolute partial WF_6 ionization cross sections for WF_5^+ (filled squares), $WF_4^+ \times 10$ (filled stars), $WF_3^+ \times 10$ (open circles), $WF_2^+ \times 10$ (filled triangles), $WF^+ \times 10$ (open triangles), $W^+ \times 10$ (filled circles), and F^+ (filled diamonds) as a function of electron energy up to 200 eV.

The numerical values of the partial ionization cross sections for the formation of singly charged ions, the partial counting ionization cross sections for the formation of doubly charged ions, and the total ionization cross section (the charge weighted sum of all partial cross sections) as a function of the energy of the ionizing electrons from threshold to 900 eV are given in Table 1. The corresponding cross-section curves of the singly and doubly charged ions are shown in Figs. 2 and 3 from threshold to 200 eV. The total WF_6 ionization cross section is shown in Fig. 4 up to 900 eV along with the total single WF_6 ionization cross section and the total WF_6 counting ionization cross section. The cross section curves of all ions show a very similar shape as a function of impact energy. The cross sections increase rapidly from threshold to a maximum and then decrease gradually towards higher impact energy. None of the cross section curves displays any indication of the low-energy structures that were found in the case of $TiCl_4$ [8]. The maximum for the singly charged ions (Fig. 2) was found to be in the range between 50 and 100 eV. The only exceptions are the W^+

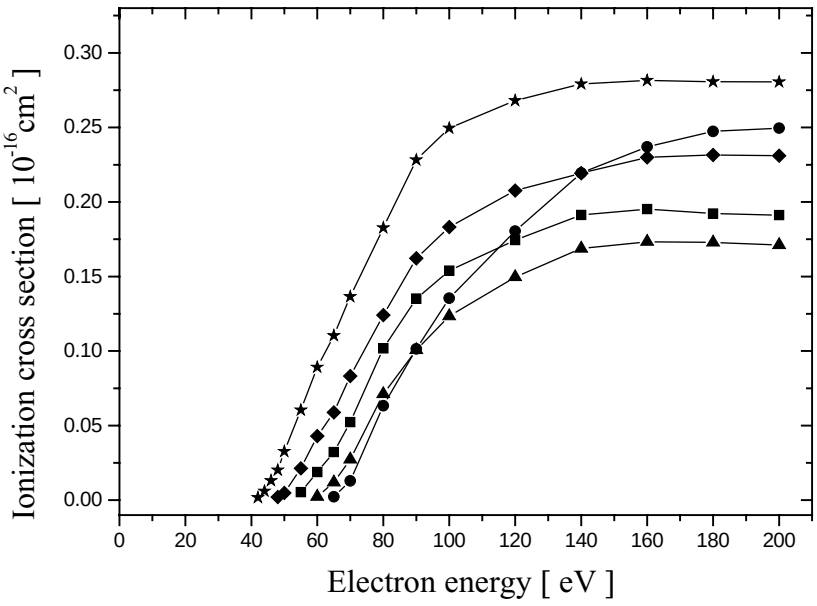

Fig. 3. Absolute partial WF_6 ionization cross sections for WF_4^{++} (filled stars), WF_3^{++} (filled diamonds), WF_2^{++} (filled squares), WF^{++} (filled triangles), and W^{++} (filled circles) as a function of electron energy up to 200 eV.

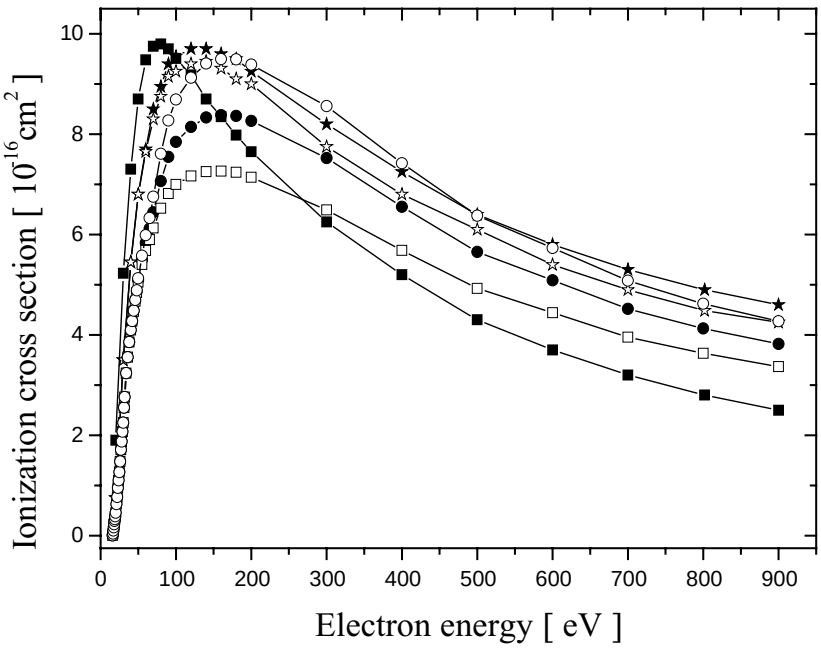

Fig. 4. Present absolute total WF_6 ionization cross section (open circles), present absolute total single WF_6 ionization cross section (open squares), present absolute total counting WF_6 ionization cross section (filled circles), calculated absolute total single WF_6 ionization cross section [18] (filled squares), and two calculated absolute total counting WF_6 ionization cross section [19] (filled and open stars) as a function of electron energy up to 900 eV.

and F^+ ionization cross sections which reach their maximum value at 200 eV. It is obvious from the cross section curves shown in Figs. 2 and 3 that dissociative ionization is the dominant process in the entire range of impact energies. We found only a very weak ion signal attributable to the formation of the $WF_6{}^+$ parent ion at very high WF_6 pressure and at electron currents that were higher than those typically employed in our measurements. The largest maximum cross-section value was obtained for the $WF_5{}^+$ fragment ion, 3.92×10^{-16} cm^2 at 120 eV. This ion accounts for about 43% of the total ionization cross section of WF_6 at 120 eV. The ion spectrum in the lower energy region, which is of special interest for low-temperature plasma technology, changes with increasing impact energy due to the different appearance energies for the various ions (Fig. 2), but is also dominated by $WF_5{}^+$. For example, $WF_5{}^+$ accounts for 99% of the total ionization cross-section value at 20 eV and for 83% at 30 eV. We note, that the cross section curves of the fragment ions $WF_4{}^+$, $WF_3{}^+$ $WF_2{}^+$ WF^+, and W^+ in Fig. 2 were multiplied by a factor of 10 for clarity of presentation.

Doubly charged ions appear at energies above 42 eV and show the largest cross section values in the energy range between 150 and 200 eV (see Table 1 and Fig. 3). All maximum cross section values are more than one order of magnitude lower compared with the maximum $WF_5{}^+$ cross section. The charge weighted sum of all doubly charged fragment ions accounts for about 21% of the total ionization cross section of WF_6 at 120 eV. The contribution to the total WF_6 ionization cross section arising from the formation of doubly charged ions is larger than for most molecules [17]. The total ionization cross-section curve of tungsten hexafluoride (last column of Table 1) is derived as the charge weighted sum of the twelve partial ionization cross sections reported here and is shown in Fig. 4. The curve exhibits a maximum at 160 eV with a peak value of 9.5×10^{-16} cm^2. Furthermore, Fig. 4 shows the comparison of various experimentally determined and calculated cross sections available for WF_6. The total single ionization cross section of WF_6 was calculated using the DM formalism [18]. The level of agreement with the experimental total single cross section is not very satisfactory below 150 eV. The calculated cross section rises faster as a function of electron energy and shows a relative sharp peak at 80 eV. At higher impact energies, the measured values exceed the calculated cross section as the calculated cross section declines faster with increasing impact energy as the measured cross section. This high-energy behavior of the DM cross section is not atypical and a consequence of the Gryzinski-type energy dependence used in this model. More recently, Deutsch et al. [20] have modified the DM formula and incorporated the quantum mechanically "correct" high-energy dependence. The other two calculated cross sections curves in Fig. 4 were obtained with two variants of the BEB method [19]. Both curves represent the total counting ionization cross section of WF_6. A comparison of the BEB cross sections with our experimental data shows a much better agreement in terms of the cross section shape and in terms of the absolute cross section values. The experimental cross-section values again are lower than both calculated cross sections in the entire energy range. The deviation between the BEB results and the experimental data decreases with increasing energy. Overall, the level of agreement between the experimental data and the BEB calcula-

tions is of the order of the experimental uncertainty of 15% above 100 eV.

4. Conclusions

We measured the absolute partial electron ionization cross sections for the WF_6 molecule using a time-of-flight mass spectrometric technique. The mass spectrum at 70 eV is in good agreement with known mass spectral cracking patterns of WF_6 for the higher ion masses. Differences with previously published data at lower ion masses can be explained in terms of a less than 100% ion collection efficiency for ions formed with excess kinetic energy, which may have affected the earlier measurements. A complete set of the absolute ionization cross sections for the formation of all positive ions from WF_6 was determined in the energy range from threshold to 900 eV. Dissociative ionization with the generation of WF_5^+ was found to be the dominant process. The comparison of the experimental data with available theoretical predictions shows a much better agreement than what was obtained before [7]. The absolute cross-section values measured here are indispensable for a microscopic understanding and the detailed modeling of the plasma chemical processes in WF_6-containing plasmas. The data presented here are also important for the critical evaluation of mass spectrometric plasma diagnostics data.

Acknowledgements

One of us (K.B.) wishes to acknowledge financial support of this work from the U.S. Department of Energy, Office of Science, Office of Basic Energy Sciences.

References

[1] P. Colpo, T. Meziani, P. Sauvageot, G. Ceccone, P.N. Gibson, F. Rossi, P. Monge-Cadet, J. Vac. Sci. Technol. A 20 (5) (2002) 1632.
[2] M.F. Bain, B.M. Armstrong, H.S. Gamble, J. Phys. IV 9 (1999) 827.
[3] T. Noma, K.S. Seol, M. Fujimaki, Y. Ohki, J. Appl. Phys. 85 (12) (1999) 8423.
[4] R. Ecke, S.E. Schulz, M. Hecker, T. Gessner, Microelectr. Eng. 64 (2002) 261.
[5] H. Li, S. Jin, H. Bender, F. Lanckmans, I. Heyvaert, K. Maex, L. Froyen, J. Vac. Sci. Technol. B 18 (1) (2000) 242.
[6] K.K. Lai, A.W. Mak, T.P. Wendling, P. Jian, B. Hathcock, Thin Solid Films 332 (1998) 329.
[7] R. Basner, M. Schmidt, H. Deutsch, Measurement of the electron ionization of tungsten hexafluoride. In: Proceedings of the 45th Annual Gaseous Electronics Conference, Boston, 1992, p. 181.
[8] R. Basner, M. Schmidt, K. Becker, V. Tarnovsky, H. Deutsch, Thin Solid Films 374 (2000) 291.
[9] R. Basner, M. Schmidt, E. Denisov, K. Becker, H. Deutsch, J. Chem. Phys. 114 (2001) 1170.
[10] R. Basner, M. Schmidt, E. Denisov, P. Lopata, K. Becker, H. Deutsch, Int. J. Mass Spectrom. 214 (2002) 365.
[11] R. Rejoub, B.G. Lindsay, R.F. Stebbings, Phys. Rev. A 65 (2002) 042713.
[12] D.R. Lide (Ed.), CRC Handbook of Chemistry and Physics, CRC Press, Boca Raton, FL, 2001/2002.
[13] NIST Database (webbook.nist.gov/chemistry/form-ser.html).
[14] R. Basner, M. Schmidt, V. Tarnovsky, K. Becker, H. Deutsch, Int. J. Mass Spectrom. Ion Proc. 171 (1997) 83.
[15] R. Basner, R. Foest, M. Schmidt, K. Becker, H. Deutsch, Int. J. Mass Spectrom. 176 (1998) 245.
[16] H.M. Rosenstock, K. Draxl, B.W. Steiner, J.T. Herron, J. Phys. Chem. Ref. Data 6 (Suppl. 1) (1977) I-344.
[17] T.D. Märk, G.H. Dunn (Eds.), Electron Impact Ionization, Springer-Verlag, Vienna, 1985.
[18] M. Probst, H. Deutsch, K. Becker, T.D. Märk, Int. J. Mass Spectrom. 206 (2001) 13.
[19] W.M. Huo, Y.-K. Kim, Chem. Phys. Lett. 319 (2000) 576.
[20] H. Deutsch, P. Scheier, K. Becker, T.D. Märk, Int. J. Mass Spectrom. 233 (2004) 13.